Molecular Microbiology (2012) 86(6), 1318–1333 ■
doi:10.1111/mmi.12071
First published online 9 November 2012

Variation of the folding and dynamics of the *Escherichia coli* chromosome with growth conditions

Nastaran Hadizadeh Yazdi,[1]* Calin C. Guet,[2] Reid C. Johnson[3] and John F. Marko[1,4]
[1]*Department of Physics & Astronomy, Northwestern University, Evanston, IL 60208, USA.*
[2]*Institute of Science and Technology Austria, A-3400 Klosterneuburg, Austria.*
[3]*Department of Biological Chemistry, David Geffen School of Medicine, University of California, Los Angeles, Los Angeles, CA 90095, USA.*
[4]*Department of Molecular Biosciences, Northwestern University, Evanston, IL 60208, USA.*

Summary

We examine whether the *Escherichia coli* chromosome is folded into a self-adherent nucleoprotein complex, or alternately is a confined but otherwise unconstrained self-avoiding polymer. We address this through *in vivo* visualization, using an inducible GFP fusion to the nucleoid-associated protein Fis to non-specifically decorate the entire chromosome. For a range of different growth conditions, the chromosome is a compact structure that does not fill the volume of the cell, and which moves from the new pole to the cell centre. During rapid growth, chromosome segregation occurs well before cell division, with daughter chromosomes coupled by a thin inter-daughter filament before complete segregation, whereas during slow growth chromosomes stay adjacent until cell division occurs. Image correlation analysis indicates that sub-nucleoid structure is stable on a 1 min timescale, comparable to the timescale for redistribution time measured for GFP–Fis after photobleaching. Optical deconvolution and writhe calculation analysis indicate that the nucleoid has a large-scale coiled organization rather than being an amorphous mass. Our observations are consistent with the chromosome having a self-adherent filament organization.

Accepted 14 October, 2012. *For correspondence. E-mail n-hadizadeh@northwestern.edu; Tel. (+1) 847 467 1187; Fax (+1) 847 467 1380.

Introduction

Our knowledge of the scheme by which the bacterial chromosome is physically organized and folded is at best incomplete. Although major advances have been made in visualizing specific genetic loci inside bacterial cells, the mechanisms underlying bacterial chromosome folding and how those mechanisms are coupled to segregation of replicated chromosomes remain poorly understood (Browning *et al.*, 2010; Wang *et al.*, 2011). A prevailing view is that the DNA in bacterial chromosomes is organized into independent supercoiled 'domains' of roughly 10 kb size (Postow *et al.*, 2004; Deng *et al.*, 2005), but historically there has often been a bias towards supposing a minimal 'random polymer' organization of the chromosome inside the cell (Browning *et al.*, 2010; Wiggins *et al.*, 2010).

However, over the past 10 years several locus-mapping experiments have established that during relatively slow growth where there is one complete cycle of DNA replication per cell division, the *Escherichia coli* chromosome is at large scales arranged in an extended 'linear' conformation inside the cell (Niki *et al.*, 2000; Bates and Kleckner, 2005; Nielsen *et al.*, 2006; X. Wang *et al.*, 2006; Wiggins *et al.*, 2010); a similar arrangement has been observed for *Caulobacter crescentus* (Viollier *et al.*, 2004) and other rod-shaped bacteria (Toro and Shapiro, 2010).

While this linear organization might be taken to indicate a spatially organized, folded chromosome conformation, theoretical work of Jun and Mulder (2006) has suggested that this could be a consequence of cylindrical confinement and otherwise random polymer behaviour of the bacterial 'chromatin'. The mechanism underlying the model of Jun and Mulder is crowding (Pelletier *et al.*, 2012): rather like train cars in a tunnel, successive regions of the chromosome are forced to occupy successive positions along the cell interior simply due to the filling of available space (Daoud and Degennes, 1977; de Gennes, 1979). As DNA replication occurs, Jun and Mulder have shown that for the same reason the two replicating chromosomes will separate from one another along the length of the cell.

While appealing from the point of view of economy, this confined random polymer model has been challenged by experiments which measured the variation in position of specific loci across cell populations (Wiggins *et al.*, 2010). The resulting position fluctuation values are less than

might be expected from a random polymer organization, leading Wiggins *et al.* (2010) to conclude that there must be an underlying filamentous organization of the chromosome, perhaps with supercoiled domains extended from a central, well-self-attached nucleoid core. In this model, the observed linear organization of chromosome loci is attributed to the underlying filamentous structure.

A fact which has not been explicitly addressed in either of these models of large-scale nucleoid organization is the role of the large numbers of non-specifically binding nucleoid-associated proteins (NAPs) found in bacterial cells, including HU, IHF, H-NS and Fis in growing *E. coli* (Rimsky and Travers, 2011). Single-molecule experiments have observed NAPs to be capable of organizing large DNA molecules into compacted and DNA-looped domains (Dame *et al.*, 2000; 2006; Ali *et al.*, 2001; van Noort *et al.*, 2004; Skoko *et al.*, 2006; Liu *et al.*, 2010; Lim *et al.*, 2012). The large numbers of NAPs found *in vivo* are suggestive of them having some role in spatially organizing the chromosome, and perhaps indirectly in the mediation of chromosome segregation.

In addition to the NAPs, smaller numbers of DNA-linking bacterial 'condensin' complexes (MukBEF in *E. coli*), which are able to trap loops along DNA (Cui *et al.*, 2008), provide a mechanism for further compaction of the nucleoid (Q. Wang *et al.*, 2006; She *et al.*, 2007). Finally, different protein species are bound to different 'macrodomains' of the *E. coli* nucleoid (Mercier *et al.*, 2008; Dame *et al.*, 2011), providing evidence for sequence-controlled folding of different chromosomal regions. Recent work has solidified our understanding of how sequence-specific protein–DNA interactions give rise to formation of a macrodomain involving the terminus region of the chromosome, which appears to play a role in chromosome segregation (Espeli *et al.*, 2012; Thiel *et al.*, 2012). NAPs, condensins and macrodomain organizers all likely contribute to compaction of the chromosome along its length, which can provide the basis for a mechanism of chromosome segregation, irrespective of confinement effects (Marko, 2009; 2011).

Having framed two possibilities, of either 'confined random polymer' or a 'filamentous folded' chromosome organization, one can ask what might be the qualitative observable differences between them. First and foremost, the confined random polymer model, being based on steric exclusion, indicates that the chromosome should fill the available space in the cell. While the definition of 'available space' might be difficult to draw precisely due to crowding and other confinement effects (Valkenburg and Woldringh, 1984; Zimmerman and Trach, 1991; Zimmerman and Murphy, 1996; Mondal *et al.*, 2011), the confined random polymer picture quite strongly suggests that replicated chromosomes should be adjacent, precisely because adjacent chromosome domains are indistinct from adjacent domains of different chromosomes. On the other hand, a folded chromosome might be expected to be significantly smaller than the cell, to have observable and persistent substructure or folding patterns, and to display segregation dynamics where replicated chromosomes are observed to occupy different regions of one cell.

We reasoned that the question of which of these behaviours is displayed by the *E. coli* nucleoid could be addressed by observation of the global chromosome structure in live cells, where the dynamics of structure and positioning of the chromosome as a whole could be followed in real time. To visualize the chromosome we constructed strains of *E. coli* carrying a quantitatively inducible gene for a fusion of green fluorescent protein (GFP) to the major NAP Fis (GFP–Fis). Fis binds DNA tightly (Shao *et al.*, 2008; Stella *et al.*, 2010; Graham *et al.*, 2011; Xiao *et al.*, 2011), and is distributed throughout the chromosome (Grainger *et al.*, 2006; Cho *et al.*, 2008; Kahramanoglou *et al.*, 2011), making it a good choice for this type of experiment. In this controllable system, induction of GFP–Fis at relatively low levels enables clear nucleoid visualization, without altering cell growth. Our observations of chromosome morphology and positioning dynamics indicate that in all growth conditions studied, the chromosome is a self-adherent, folded object with persistent small-scale features, including an overall coiled shape. Also, our time-lapse measurements of the nucleoid position shows that for rapid growth, chromosome positioning in the cell centre and segregation of replicated chromosomes are events which are well separated in time from cell division itself. However, for slow growth conditions, we find that the replicated chromosomes do remain adjacent until immediately before cell division.

Results

Induction of GFP–Fis *does not alter cell growth rates*

Experiments on live *E. coli* cells were carried out using observations of 'linear microcolonies', lines of growing bacteria organized by grooves on a thin slice of agarose gel used to confine the cells against a cover glass. The cells were thus confined, yet obtained nutrients from the cell growth buffer that permeates the agarose (Fig. 1A). The number of cells was small enough that their growth was not perturbed by build-up of waste products on the few-hour timescale of typical experiments. This technique allowed us to track cells under different growth conditions and to visualize the chromosomes as cells grow and divide.

Measurements of single cell doubling times and bulk growth rates, for different levels of induction, show that the level of GFP–Fis expression up to full induction by 1 mM IPTG (Fig. S1) does not perturb cell growth (Fig. S2). Measurements of cellular GFP–Fis levels also show that the number of fusion proteins expressed under our experimental conditions is significantly lower than physiological

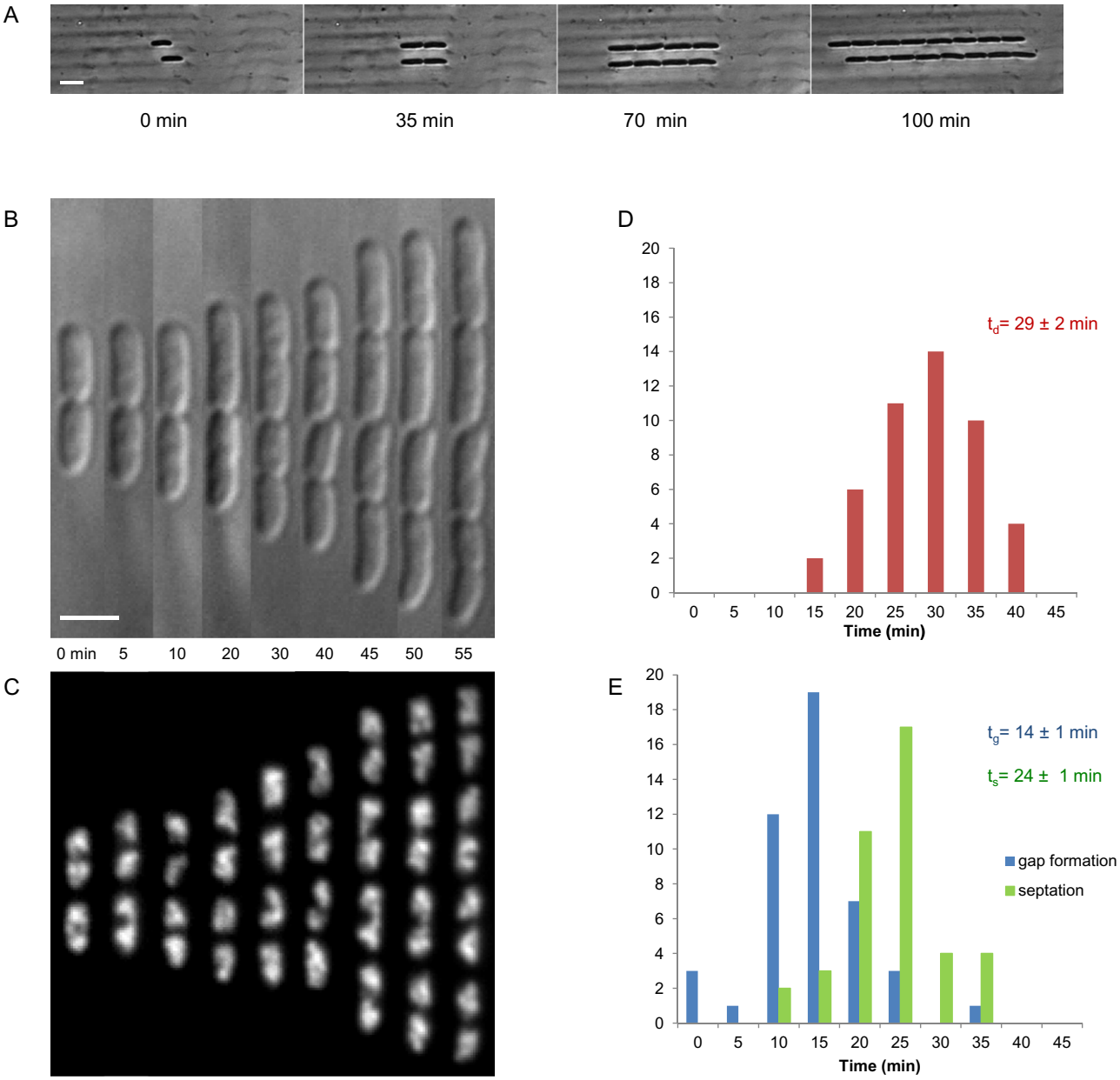

Fig. 1. Rapid growth of *E. coli* in LB.
A, B. (A) Bright field images and (B) differential interference contrast (DIC) images of cells growing and dividing in grooves under LB-agarose pad dividing approximately every 30 min at 30°C.
C. Fluorescence images of chromosomes in cells expressing GFP–Fis during rapid growth showing the morphological changes of the nucleoids as they become bilobed and segregated.
D. Histogram of doubling times ($n = 50$) for a typical induction level (0.5 mM IPTG).
E. Histogram of septum and gap formation times ($n = 50$) indicating the time difference between the two events. Bar is 2 μm.

levels in LB (Fig. S1). Similar measurements conducted for cells growing in minimal media where less Fis is present showed that induction of GFP–Fis did not significantly perturb the total number of Fis plus GFP–Fis molecules (expression of wild-type Fis was reduced in response to induction of GFP–Fis, Fig. S1), and also that there was no significant difference in growth rate over a similar range of IPTG concentration (Fig. S3).

Splitting, thinning and separation of compacted daughter nucleoids occur as chromosome segregation proceeds during rapid growth in LB

Rapidly growing cells under an LB-agarose pad were visualized while going through multiple cell division cycles with doubling time of approximately 30 min at 30°C (Fig. 1A and B). Time-lapse fluorescence images taken

with a 0.5 s exposure time did not affect cell viability appreciably (10% increase in cell-doubling time compared to numbers in Fig. S2). The fluorescence images show how the overall morphology of the nucleoid changes as it replicates and segregates. During rapid growth, where the doubling time is shorter than the replication time and there are multiple rounds of replication (Cooper and Helmstetter, 1968; Nielsen *et al*., 2007), we observe chromosomes to be organized into multiple domains with a complex geometrical organization (Fig. 1C). The nucleoids as a whole undergo a global splitting and separation well before the cells themselves divide.

As shown in Fig. 1C, the nucleoid starts to become bilobed early in the cell division cycle (5 min and 40 min). The two daughter nucleoids subsequently segregate (Fig. 1C, 10 min and 50 min), with a large gap (approximately 20% of the cell length) forming between them roughly 15 min before the septum is first observed (Fig. 1E). We also observed that the segregating nucleoids are highly self-compacted, with trailing regions of thin nucleoids between them just before segregation is complete (Fig. 1C, 45 and 50 min frames). These observations indicate that during rapid growth, chromosomes are compact structures with well-defined shape, and that replicated chromosomes segregate well before cell division.

We have checked that one can observe similar patterns using a different DNA-binding protein. Using expression of inducible *Anabaena* HU fused to GFP, we have verified that during rapid growth in LB, the same general nucleoid patterns are observed except for the haze around the nucleoids consistent with the weaker DNA-binding affinity of HU relative to that of Fis (Swinger and Rice, 2004; Graham *et al*., 2011; Xiao *et al*., 2011) (Fig. S4).

Chromosome geometry is stable at optical length scales on a minute-long timescale during rapid growth in LB

Time-lapse fluorescence images of the cells growing rapidly in LB show a dynamic domain structure of the nucleoid throughout the cell cycle (Fig. 1C). Observation of these domain structures and an overall shape for the nucleoids for a range of exposure times (Fig. S5) indicate that chromosome domain organization at length scales observable by imaging microscopy (> 0.2 μm) is not rapidly changing; images show similar geometrical patterns for exposure times from 0.05 to 3 s. Thus, there is no appreciable smearing at optically observable length scales by our nominal exposure time of 0.5 s.

In order to estimate the timescale over which the domain structures are stable, we acquired time series of images (0.5 s exposure time) with one image recorded every 10 s. These rapid sequence images (Fig. 2A) show that the overall nucleoid shape (two segregating daughter nucleoids with a thin trailing region between them) is stable over a few-minute timescale, while there is some variation in the sub-nucleoid patterns (shape of the top and bottom parts of the nucleoid) at a smaller timescale, suggesting that fluctuations of the observed domain structures are faster at shorter length scales but slow enough to not cause motion blurring in our images with a 0.5 s exposure time. A qualitative analysis of the rapid sequence images of 10 cells (see additional time sequences of images in Fig. S6) indicated that on average, the overall geometry of the chromosome is stable over a 90 ± 30 s timescale. We also note that time-averaging the images for 2 min causes only a small amount of motion blurring, with nucleoid substructure still evident (Fig. S6).

To determine the sub-nucleoid structural rearrangement timescale more quantitatively, we also did a correlation analysis of the rapid sequence images, where the average autocorrelation coefficient of the total intensity in sub-nucleoid regions (0.5 μm-wide square regions) was calculated over time and averaged over the nucleoid. The average correlation function was then fit by an exponential (decaying to a constant); the exponential decay ($1/e$) time was taken to be the correlation time (Fig. 2B). The correlation analysis was performed for 15 cells resulting in an average correlation time of 75 ± 15 s. This result further confirms that the nucleoid shape is stable over a timescale much longer than our image acquisition timescale of less than 1 s.

Chromosomes have a linear, filamentous structure during slow growth in M9 minimal medium

In order to investigate the effect of growth conditions on nucleoid morphology, we also visualized cells growing slower in M9 minimal medium supplemented with glycerol. The cell doubling time under these conditions is approximately 80 min (Fig. 3C), which is longer than one complete replication period (Wang *et al*., 2005). As shown in Fig. 3A, cells grown in M9 glycerol are thinner and longer compared to rapidly growing cells in LB. The nucleoid also has a more elongated organization (Fig. 3B). As the cell cycle proceeds, the cell elongates, and the nucleoid becomes longer. Variations in GFP intensity suggestive of domain structure ('blobs') are present, and separation of nucleoids occurs at nearly the same time as septation, slightly preceding cell division (Fig. 3D). These observations suggest that the M9 nucleoid also has a definite folding pattern (the narrow linear organization and blobs) but that, in contrast to LB growth, the nucleoids stay adjacent until septation starts and the cell itself divides.

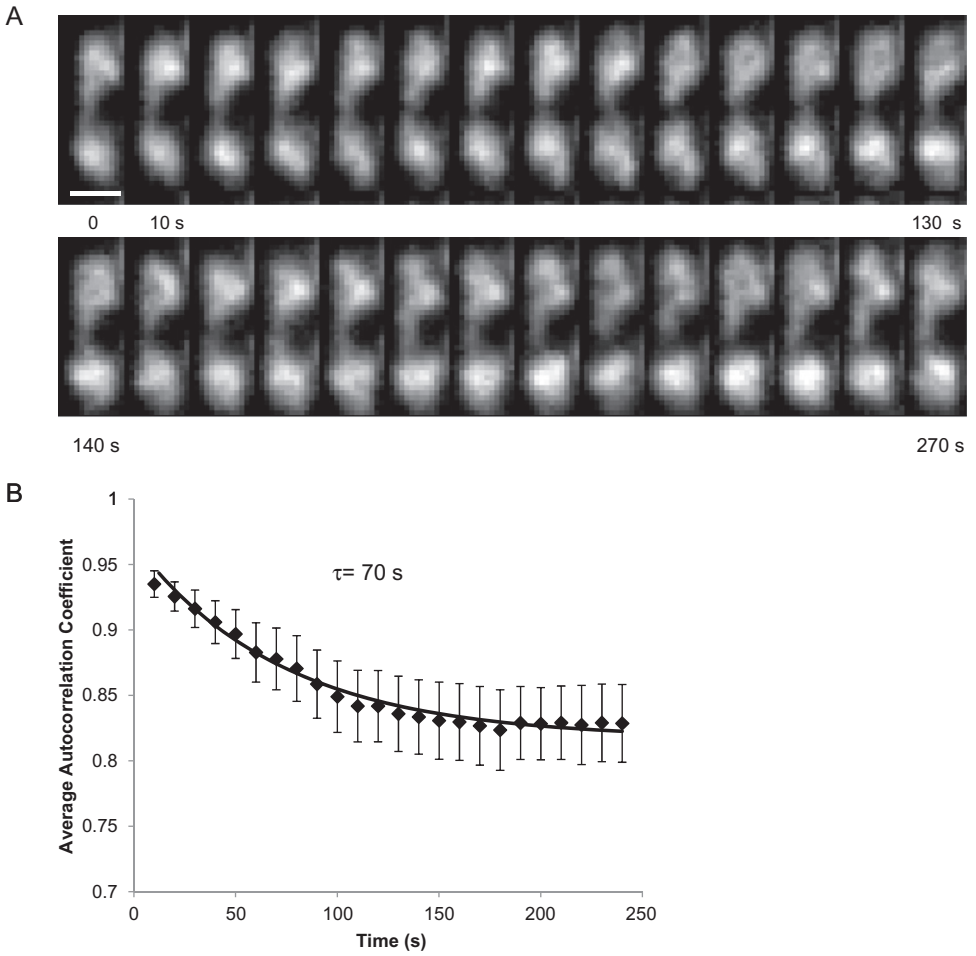

Fig. 2. Dynamics of chromosome geometry.
A. Sequence of images of a segregating nucleoid in a cell expressing GFP–Fis and growing under a LB-agarose pad, showing the overall geometry of the nucleoid persists over a few-minute timescale (10 s between images, 0.5 s exposure time). Bar is 1 μm.
B. The average autocorrelation function for one cell with a characteristic time of approximately 70 s, calculated for a time series of images similar to the ones in (A).

Chromosome segregation and dynamics in AB glucose-acetate and M9 glycerol minimal media are similar

To further investigate the effects of growth conditions on chromosome segregation, we also visualized cells grown in AB glucose-acetate media with a doubling time of approximately 110 min (Fig. 3G), significantly longer than one replication period (Bates and Kleckner, 2005). As shown in Fig. 3E and F, cells are slightly smaller than those growing rapidly in LB and the nucleoids are smaller and less well-defined in shape compared to both LB and M9

Fig. 3. Slow growth of *E. coli* cells.
A. DIC images of cells expressing GFP–Fis growing in grooves under M9 glycerol-agarose pad, dividing approximately every 80 min at 30°C.
B. Fluorescence images of chromosomes in cells showing that chromosomes maintain a linear organization, taking the form of a filament during slow growth in M9. As the cell cycle proceeds, the chromosome filament gradually becomes longer and finally splits at septation (75 min and 85 min frame).
C. Histogram of doubling times ($n = 40$) for a typical induction level (0.5 mM IPTG).
D. Histogram of septum and gap formation times ($n = 40$) indicating that on average there is no discernible time difference between the two events.
E. DIC images of cells growing under AB glucose-acetate agarose pad, dividing approximately every 110 min at 30°C.
F. Fluorescence images of chromosomes in cells expressing GFP–Fis during slow growth in AB, showing the segregation does not occur until cell division.
G. Histogram of doubling times ($n = 50$) for a typical induction level (0.5 mM IPTG).
H. Histogram of septum and gap formation times ($n = 50$) indicating that gaps between the daughter nucleoids do not appear until septum formation or after that. Bar is 2 μm.

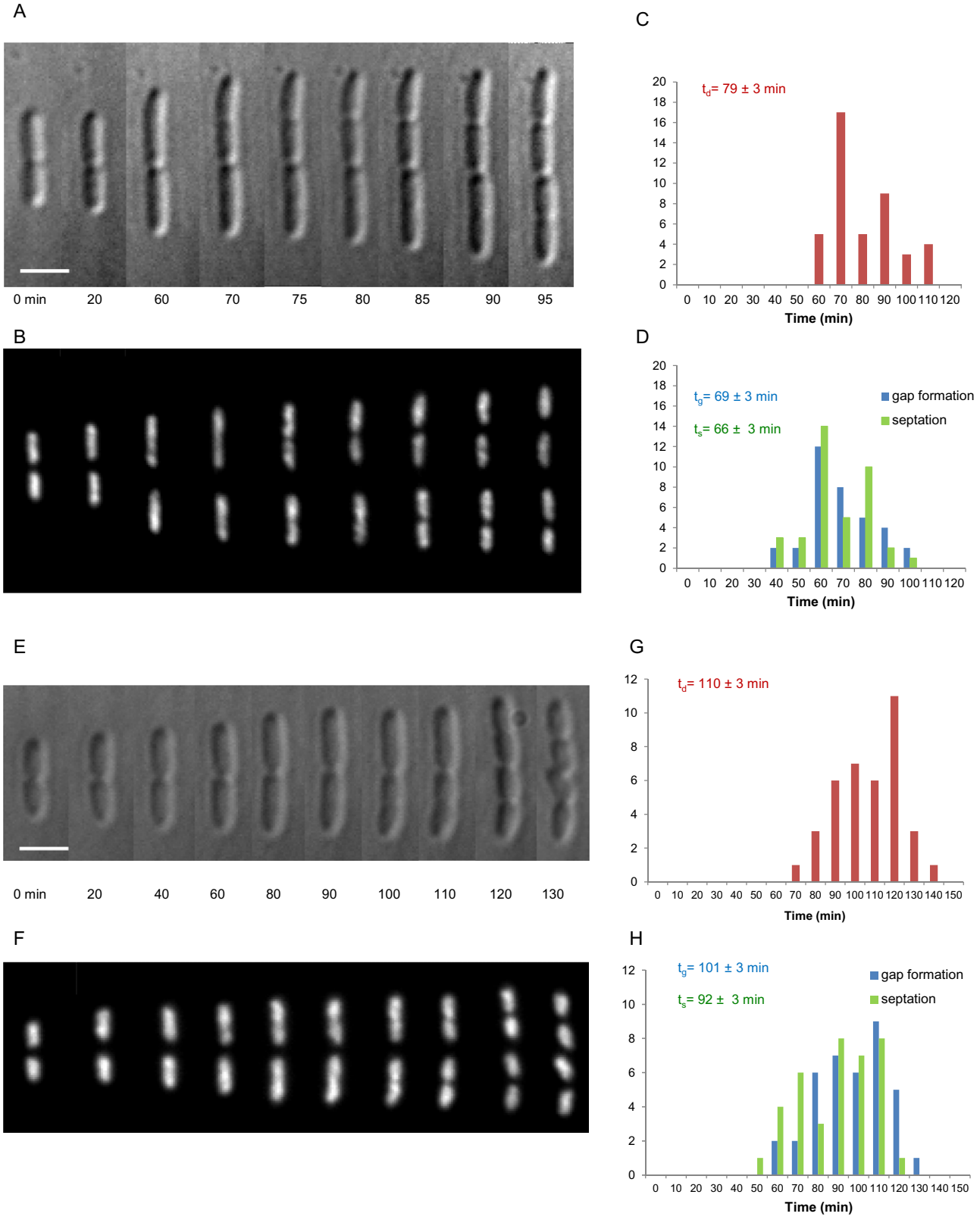
A
0 min
20
60
70
75
80
85
90
95
B
C
t_d= 79 ± 3 min
Time (min)
D
t_g= 69 ± 3 min
t_s= 66 ± 3 min
gap formation
septation
Time (min)
E
0 min
20
40
60
80
90
100
110
120
130
F
G
t_d= 110 ± 3 min
Time (min)
H
t_g= 101 ± 3 min
t_s= 92 ± 3 min
gap formation
septation
Time (min)

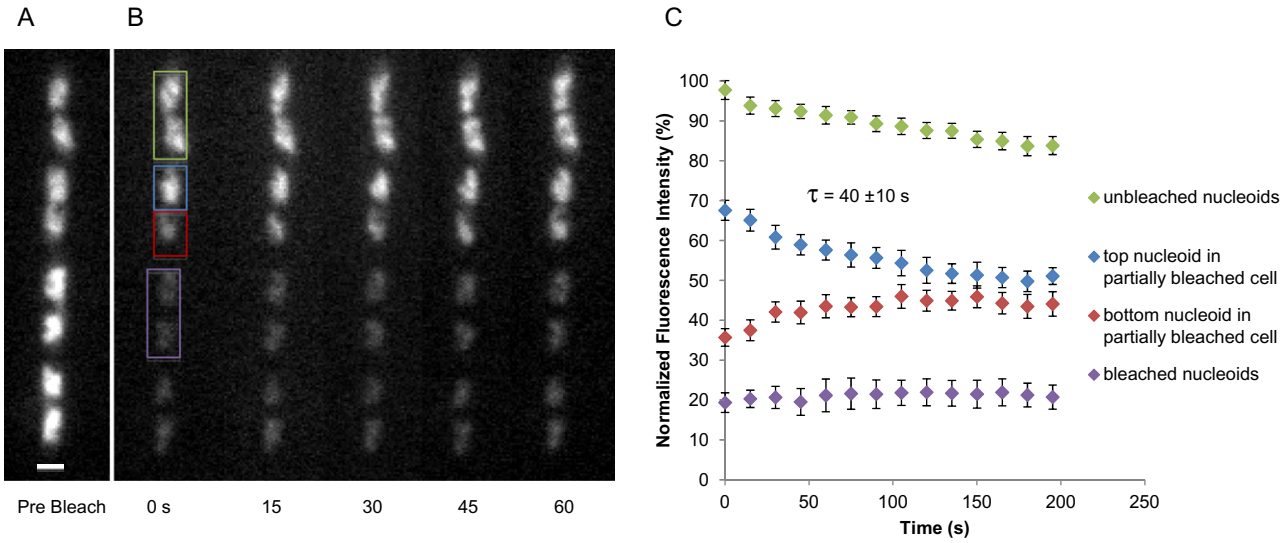

Fig. 4. FRAP analysis of GFP–Fis dynamics during rapid growth in LB.
A. Fluorescence image of nucleoids before bleaching.
B. Time-lapse images after bleaching showing the recovery of the bleached portion of the half-bleached cell. Bar is 1 μm.
C. Fluorescence intensity profiles showing that the nucleoid in a partially bleached cell reaches an intermediate intensity level with an average characteristic time of 40 ± 10 s ($n = 7$ cells analysed). Fluorescence intensity profiles of the unbleached and evenly bleached nucleoids show relatively constant intensity levels.

glycerol media. However, we do observe apparent domain structure along the nucleoid, as well as onset of separation of the two halves of the nucleoid as the cell cycle progresses. Time-lapse images in Fig. 3F show that in AB glucose-acetate, nucleoids become bilobed approximately 60 min into the cell division cycle, but the segregating daughter nucleoids stay very close to each other until halfway through septum constriction and just before cell division (Fig. 3H), similar to the pattern seen in slower growth in M9 glycerol.

Similar patterns were also observed in cells expressing *Anabaena* HU–GFP during slow growth in M9 glycerol and AB glucose-acetate (Fig. S7); however, the nucleoid substructures are not as visible as in cells expressing GFP–Fis, again possibly due to the weaker DNA-binding affinity of the HU proteins relative to Fis.

The time-lapse fluorescence images of the cells during slow growth show how the apparent domain structure of the nucleoids changes throughout the cell cycle. In order to have an estimate of the dynamics of these structures and compare them to the case of rapid growth, we acquired sequences of images of the GFP–Fis nucleoids during slow growth (one image per 10 s with a 0.25 s exposure time, in M9 glycerol and AB glucose-acetate, see Fig. S8). The image sequences indicate that the timescale of the domain structure dynamics is faster than we observed for rapid growth. Image correlation analysis also indicates that during slow growth, the nucleoid shape is stable on a slightly shorter timescale than observed for growth in LB (40 ± 10 s for cells in M9 glycerol, $n = 15$; 55 ± 10 s for cells grown in AB glucose-acetate, $n = 15$).

Fis *shows fluorescence recovery after photobleaching on approximately 1 min timescale*

Having found that the geometrical shape of the chromosome persists over a few-minute timescale, with no optically observable changes due to motion blurring at 0.05 to 3 s times (Fig. S5), we were curious whether the GFP–Fis we were using for the visualization was mobile on a shorter or longer timescale than that associated with the chromosome motion. In order to investigate mobility of the expressed GFP–Fis in cells growing in LB, we used fluorescence recovery after photobleaching (FRAP). Half of the nucleoid in a single cell was partially photobleached, generating an intensity gradient along the long axis of the cell; subsequently fluorescence intensities in both halves of the cell were monitored (Fig. 4).

The recovery curves in Fig. 4B show normalized fluorescence intensity for both halves of partially bleached nucleoid at each time point, indicating that the nucleoid reaches an intermediate intensity level with an average characteristic time of 40 ± 10 s ($n = 7$), while the overall shape of the nucleoid stays more or less the same during the recovery time (Fig. 4A). Fluorescence intensities of the unbleached and evenly bleached nucleoids were also monitored at the same time which showed a relatively constant intensity level (Fig. 4B), indicating that the recovery is not due to synthesis of new fluorescent proteins

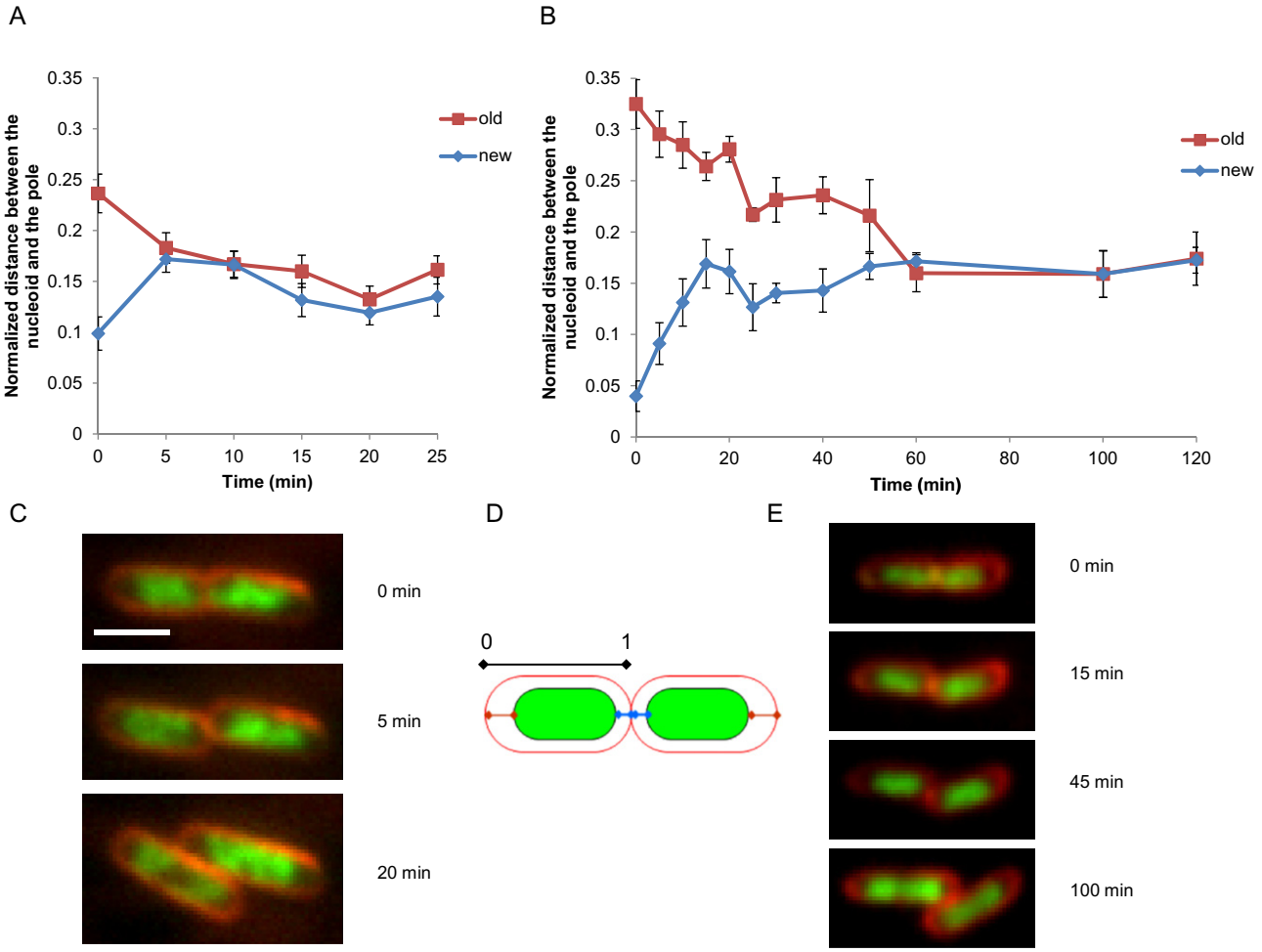

Fig. 5. Time-lapse measurements of nucleoid positioning.
A, B. (A) Dynamic positioning of the nucleoid for rapid growth in LB with doubling time of ~35 min and (B) slow growth in AB minimal medium with doubling time of ~130 min (~20% increase in doubling times for both cases, due to more exposure for visualization of the membrane). Time indicates time since previous cell division; red curves indicate distance between chromosome edge and old (external) cell poles; blue curves indicate distance between chromosome edges and newly created (internal) cell poles. A strong asymmetry is seen between the positioning of chromosomes relative to old and new poles immediately following cell division. The chromosomes are subsequently translated from the new pole regions of the cell, to near the centre of the cell. Plots show average of the measurements for $n = 20$ cells in each case.
C. Membrane and the nucleoid visualized in cells (expressing GFP–Fis) growing in LB, showing nucleoids becoming symmetrically positioned in the first 5 min of the cell cycle and remain at mid-cell for the rest of the cell cycle. Bar is 2 μm.
D. A schematic drawing of an *E. coli* cell dividing and the measurements of the gaps.
E. Membrane and the nucleoid visualized in cells growing slowly in AB glucose-acetate showing nucleoid becoming symmetrically positioned later in the cell cycle.

but rather is due to the mobility and intermixing of the proteins in the cell. The GFP–Fis proteins can move freely throughout the cell, indicating that the entire cell is one diffusion-permeated compartment. The redistribution of GFP–Fis on the nucleoid is much slower than our typical imaging times, and comparable to the timescale at which the whole chromosome is geometrically reorganized.

Chromosomes are repositioned during the first half of the cell division cycle

The previous figures used differential interference contrast (DIC) images of cells to estimate the time of cell division. We also used a membrane stain to more precisely study the relative spatial dynamics of the membrane and nucleoid (Fig. S9). Time-lapse measurements of the nucleoid position (Fig. 5A, B and D) show that the chromosome starts out closer to the cell division plane immediately following division as might be expected, and then moves away from the new pole to reposition at the middle of the cell, with cytoplasmic gaps on either side. These dynamics were observed for rapid and slow growth conditions. For cells grown in LB with a doubling time of ~35 min, the nucleoid is repositioned symmetrically during the first 5 min of the cell cycle, followed by the gradual shrinking of the cytoplasmic gaps (Fig. 5C) as the nucleoid becomes

bilobed and then divides into two daughter nucleoids, and the next division occurs.

For cells grown in AB glucose-acetate with a doubling time of ~130 min, the nucleoid moves away from the new pole more quickly than it moves towards the old pole during the first 15 ± 5 min after cell division, resulting in it still being asymmetrically positioned. The cytoplasmic gaps on both sides shrink, and then their sizes remain constant while the cell grows and the nucleoid becomes longer (Fig. 5E), until 50 ± 5 min into the cell division cycle when the nucleoid becomes symmetrically positioned in the cell until the next division. These observations indicate that repositioning of the nucleoid in slow growth is delayed and involves discrete transitions.

Deconvolution analysis indicates coiled organization of the chromosome but without a definite chirality

To obtain better resolution of substructures seen in the fluorescence images of the nucleoids (Figs 1–3) and to further investigate the nucleoid organization, z-stacked fluorescence images were collected and deconvolved using constrained iterative analysis. As shown in Fig. 6, deconvolved z-stacks of images revealed coiled filamentous organization for the nucleoid in all three growth conditions. Cells grown in M9 glycerol did not show as obvious a helical structure of the nucleoid (Fig. 6E) as in the case of LB (Fig. 6B) and AB glucose-acetate (Fig. 6F), possibly due to the narrow shape of the cells grown in M9 glycerol. However, nucleoids from cells growing slowly in M9 glycerol do show a spatially modulated organization consistent with an underlying coiled shape. Measurements of the thickness of the nucleoid in the deconvolution images indicated a thickness of 0.45 ± 0.03 μm ($n = 10$) for cells grown in LB, 0.28 ± 0.02 μm ($n = 10$) for cells grown in M9 glycerol, and 0.29 ± 0.02 μm ($n = 10$) for cells grown in AB glucose-acetate. The thicker filament size during rapid growth possibly reflects the greater amount of partially replicated chromosomal DNA present in each sub-nucleoid half under such conditions.

Observation of the coiled patterns raises the question of whether there is a definite chirality to the nucleoid organization. A rough survey of the chirality by scrolling through the deconvolved z-stacks indicated that right- and left-handed coiled nucleoids occur with approximately equal frequency. In order to determine the chirality of these patterns more quantitatively, we carried out a writhe calculation analysis (Fig. 6). The z-stacked fluorescence images (Fig. 6B) were resliced perpendicular to the cell's long axis and the centre of mass in each cross section was found by identifying the local maxima in every cross section (Fig. 6C). Then the centre of mass co-ordinates were connected and smoothed to reconstruct the nucleoid path as a polygon for which we computed the writhe (Fig. 6D).

This analysis was performed for approximately 30 cells in each growth condition, resulting in writhe distributions of Gaussian shape, with peaks close to zero writhe (Fig. 6G). The standard deviation of the writhe distribution of 0.1 for all three cases suggests that there is a net helicity in the nucleoid organization irrespective of growth rate. However, the average writhe being close to zero indicates that there is not a chiral bias for the nucleoid coiling, except perhaps in the slowest-growth (AB) case, where we do find a net negative (left-handed) writhe (probability $P \sim 3 \times 10^{-5}$ for the net writhe to be positive).

Discussion

Structure and global segregation dynamics of E. coli *nucleoids depend on growth conditions*

We have presented data for *in vivo* visualization of chromosome dynamics in *E. coli* cells, using fluorescence of GFP–Fis to read out nucleoid structure. We observed that during rapid growth in LB where multiple rounds of replication occur per division cycle, chromosome segregation starts to occur well before cell division, with a large gap developing between the duplicated chromosomes. As segregation occurs, a thin extended connection remains between segregating daughter nucleoids. Overall, nucleoids of cells growing rapidly in LB display a complex geometrical organization (many small domains and/or bent filament shape, Fig. 1) suggestive of a folded and coiled nucleoid filament. The geometrical patterns we observe evolve slowly, on a minute-long timescale, at optically resolvable length scales (Fig. 2).

Our observations for rapid growth in LB are inconsistent with a simple random-coil-like polymer model, e.g. folding of the chromosome into a series of supercoiled domains which are compacted solely by external crowding effects (Jun and Mulder, 2006). In that case, we would expect the chromosome to have a diffuse and not filamentous appearance, and we would expect segregating nucleoids to be immediately adjacent, without a tendency to move far apart from one another before the cell itself divides. We also would not expect to see complex geometrical structures smaller than the whole chromosome persist for minutes or longer (Fig. 2). Finally, random-coil structures would not tend to be compacted in distinct regions of the same cytoplasmic compartment (Fig. 4) with a stretched trailing chromosome region between them, as we have observed during rapid growth in LB (Fig. 3).

It is interesting to compare our images for LB growth time-averaged for 2 min (Fig. S6) with recent stochastic optical reconstruction microscopy (STORM) images of bacterial nucleoids collected over 2 min intervals (Wang *et al.*, 2011). While our images show appreciable nucleoid substructure, the corresponding STORM images show no

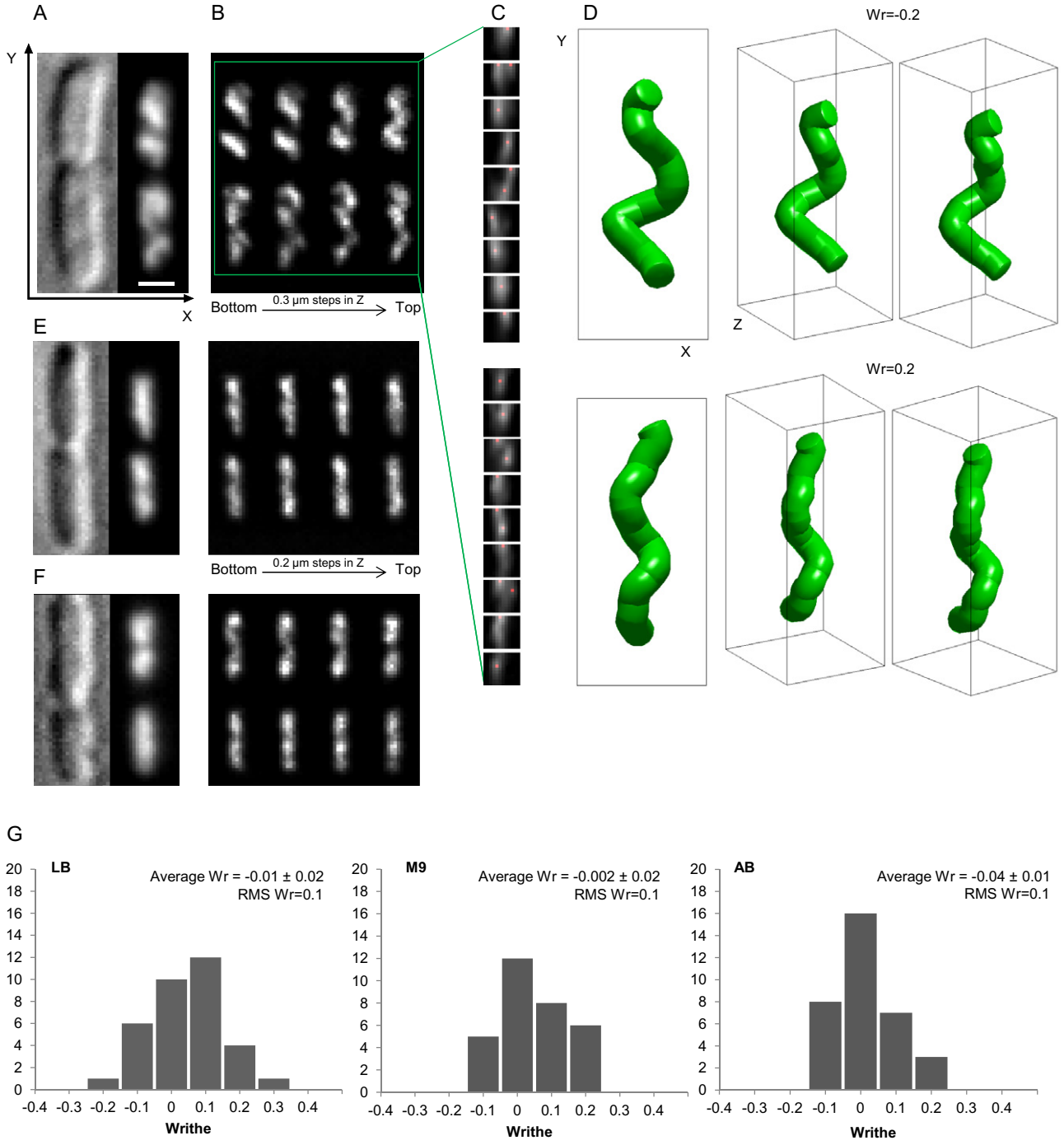

Fig. 6. Optical deconvolution and writhe calculation analysis of GFP–Fis-labelled nucleoid images.
A. DIC and florescence images of two *E. coli* cells (expressing GFP–Fis) in early stage of cell division cycle, grown in LB. Bar is 1 μm.
B. XY view of deconvolved z-stacked images of the cells showing a coiled pattern for the nucleoids.
C. Reslicing the z-stack perpendicular to the long cell axis shows XZ cross sections of the cells (not all slices shown here). Local maxima in each slice are highlighted in red.
D. XY and XYZ views ('cross-eyed' stereo pairs) of the smoothed centre of mass trajectories with calculated writhe of the nucleoids. Dimensions of the XYZ box are $1.2 \times 1.2 \times 3$ μm and the thickness of the trajectories is approximately 0.3 μm.
E, F. (E) DIC and florescence images, and deconvolved z-stacked fluorescence images of cells (expressing GFP–Fis) grown in M9 glycerol and (F) AB glucose-acetate media showing a coiled pattern for the nucleoids.
G. Writhe distributions for three different growth conditions ($n = 30$).

apparent structure. It appears that while the STORM imaging is excellent at discerning small structures such as H-NS clusters inside the nucleoid (Wang *et al*., 2011), it may not be an optimal technique for resolving the geometry of larger, three-dimensional structures such as the whole nucleoid.

In contrast to the LB results, during slow growth in M9 glycerol or in AB glucose-acetate media where only one round of replication occurs per division cycle, we found that the replicating nucleoids do stay adjacent to one another, until the cell itself divides (Fig. 3). In some cases we observed thinning of the centre of the nucleoid in accordance with previous observations of formation of 'bilobed' nucleoid patterns preceding segregation (Mason and Powelson, 1956; Bates and Kleckner, 2005; Joshi *et al*., 2011), but without the obvious stretching that we found for cells growing rapidly in LB. Nucleoids from cells growing in minimal media have much less well-defined edges, suggesting a less condensed organization than in LB, and consistent with prior observations of less nucleoid condensation in slower-growing cells (Jin and Cabrera, 2006). Functional genomics data show that under minimal media conditions almost twice as many genes are expressed compared to rich media (LB) conditions (Tao *et al*., 1999); larger number of expressed genes thus correlates with a less condensed chromosome organization. We still observe modulated and curled nucleoid structures during slow growth in M9 or AB (Fig. 6), suggestive of a definite folding pattern and inconsistent with a purely random-coil organizational scheme.

We also note that chromosome structure in rapidly growing (LB) cells can be rapidly modified, either using rifampicin, which inhibits elongation of RNAs by RNA polymerase, or using chloramphenicol, which inhibits translation by blocking peptide bond formation. Rifampicin treatment leads to rapid expansion of LB nucleoids (Cabrera *et al*., 2009) and much less expansion of M9 and AB nucleoids, which we have verified for the cells used in this work (Fig. S10). This suggests that elongating RNAs may play some role in nucleoid condensation, which is increased during rapid growth by higher RNA polymerase activity. The rifampicin decondensation also makes very clear that the nucleoid is smaller than the cell interior. Alternately, chloramphenicol treatment leads to nucleoid overcondensation (Cabrera *et al*., 2009), which again we have verified (Fig. S11), and which suggests that active ribosomes play a nucleoid-decondensing role, perhaps as a result of coupled translation and transcription of membrane proteins (Libby *et al*., 2012). These observations indicate that the LB nucleoid is in an intermediate state of condensation under normal growth conditions.

Our results indicate that in addition to crowding effects and confinement, there are other factors responsible for chromosome organization and segregation in *E. coli*. As mentioned earlier, the large number of NAPs could play a major role in folding the chromosome into a nucleoprotein filament. These DNA–protein interactions as well as plectonemic supercoiling can generate lengthwise condensation that could contribute to chromosome segregation. It is possible that the lengthwise condensation, which facilitates rapid chromosome segregation, is larger during rapid growth in *E. coli*, whereas during slow growth a lesser degree of chromosome condensation might be sufficient for slower segregation (Marko, 2009).

The nucleoid moves as a coherent object inside the cell

Time-lapse measurements of the nucleoid position in the cell (Fig. 5A and B) showed that following division, the nucleoid moves from the new-pole regions to near the centre of the cell. Similar translational nucleoid motion has been observed in a study where the origin and terminus regions were monitored during slow growth (doubling time of approximately 120 min), showing fixed positioning of those regions relative to the nucleoid but movements relative to the cell poles during this transition. This has been interpreted to indicate that origins and termini are released from their fixed cellular positions and the nucleoid is repositioned in the cell as an 'internally static unit' (Bates and Kleckner, 2005).

Our measurements of nucleoid position showed that this translation positions the nucleoid symmetrically in the cell for the rest of the cell division cycle in rapid growth. In the case of slow growth in AB the nucleoid was not centred until 50 $\pm$ 5 min into the cell cycle (Fig. 5B). The nucleoid localization transitions that we have observed during slow growth may be associated with the discrete sequential positioning of the sister origins to the opposite ends of the cell, and the proposed 'intersister snap release' (Bates and Kleckner, 2005; Joshi *et al*., 2011). The repositioning could also be driven by transport of specific macrodomains (Possoz *et al*., 2012), with the remainder of the nucleoid responding via elastic stress. These repositioning dynamics, as well as the apparent stretching of the nucleoid we observe just before cell division in LB, are suggestive of involvement of active translation of an elastic nucleoid.

E. coli *chromosomes are not simply compacted random-coil structures*

Using deconvolution analysis we observed nucleoids to have a globally coiled organization (Fig. 6). Examining the chirality using computation of writhe of the centreline of the nucleoid indicated that in one cell, both right- and left-handed turns occur resulting in a small net writhe of approximately 0.1 and an average writhe close to zero for

the cell population (Fig. 6G). The writhe distributions for the three different growth conditions show that the peak of the distribution is close to zero for rapid growth in LB and moderately slow growth in M9-glycerol, but is shifted towards negative values for the very slow AB glucose-acetate growth condition. There may be a tendency to develop large-scale negative (left-handed) chromosome writhe for slow-growth conditions. We note that our writhe analysis is cell cycle-averaged; it is possible that chromosome writhe is varying as one goes through the cell cycle.

Helical patterns of internal organization have been previously observed in *E. coli* and other bacteria. Helical organization of newly replicated DNA has been reported in *Bacillus subtilis* (Berlatzky *et al*., 2008) and spiral trajectories for nucleoids from *E. coli* have been observed in a recent study (Pelletier *et al*., 2012). Previously observed helical structures in *E. coli* have been associated with cytoskeletal and cytoskeletal-like structures, e.g. MreB, MinD, RNaseE and RNA helicase filaments (van den Ent *et al*., 2001; Kruse *et al*., 2003; Shih *et al*., 2003; Boeneman *et al*., 2009; Valencia-Burton *et al*., 2009). In a recent study, it has been shown that MreB structures rotate circumferentially around the long cell axis which could be coupled to the rotation of the cell-wall synthases (van Teeffelen *et al*., 2011). These cytoskeletal structures and the rotational movements could impose a coiled organization on the nucleoid. Alternately, it is possible that the coiled organization of the chromosome arises from DNA superhelical stress or by folding patterns imposed by NAPs (Rimsky and Travers, 2011), and that nucleoid shape controls the helical structure of the scaffold proteins. Our controllable GFP–Fis system could be used to study how chromosome folding is modified in NAP or cytoskeletal component mutants in order to determine whether the cytoskeleton shapes the nucleoid or vice versa.

E. coli *chromosomes are self-adherent objects with persistent geometrical shapes*

Our observations of chromosome dynamics in different growth conditions are consistent with a broad conclusion about *E. coli* chromosome structure. The definite shapes and positioning dynamics suggest that the chromosome is a compact, self-adhering object rather than a purely confinement-shaped random coil. We emphasize that this is not to say that the chromosome is a solid object with no random polymer fluctuations: by contrast, our picture is of a chromosome which at short scales (< 0.1 μm) is made up of randomly moving, supercoiled domains, but at longer length scales is attached to itself so as to define the nucleoid shape. These self-attachments would most likely be mediated by DNA-binding proteins able to link two double helices, e.g. bacterial condensins such as *E. coli* MukBEF (Cui *et al*., 2008), or NAPs known to be able to link DNA segments such as H-NS (Dame *et al*., 2006) or Fis (Skoko *et al*., 2006).

One can estimate the length scale and sequence length scale at which cross-links would be required in order to produce the results that we have observed. In our images, we observe a filament thickness of approximately $R = 500$ nm, which corresponds to the maximum distance that cross-links could be spaced on the nucleoid (if cross-links were spaced further than this, random-coil fluctuations of the bacterial chromatin would smooth out nucleoid structure on length scales longer than those apparent in, e.g. Fig. 6). The DNA contour length corresponding to this distance, assuming a random-coil organization at shorter scales, is approximately $L = R^2/(2A)$, where A is the DNA persistence length of roughly 50 nm. This indicates a maximum length of DNA between cross-links on the order of $L = 2500$ nm, or about 8 kb. This estimate is approximate: for example, the relevant persistence length might well be taken to be that of DNA coated by DNA-bending NAPs, possibly reducing the effective persistence length to $A \approx 25$ nm (Ali *et al*., 2001; van Noort *et al*., 2004; Skoko *et al*., 2006); this would increase our estimate of the cross-link spacing to ~16 kb. However, the conclusion that there are many self-attachment points along the chromosome with spacing on the order of 10 kb will not be altered. Notably, this characteristic length coincides with domain sizes inferred from topological analyses (Postow *et al*., 2004; Deng *et al*., 2005) and with the average spacing of NAP clusters seen in protein-occupancy landscape analyses (Vora *et al*., 2009).

It is revealing to compare the nucleoid structure correlation time of $\Delta t \approx 75$ s that we have observed at 0.5 μm length scales (Fig. 3) to the timescale expected for thermal diffusive motion of a nucleoid region of size $R = 0.5$ μm, $\Delta t = \eta R^3/(k_B T)$, where η is the viscosity and $k_B T = 4 \times 10^{-21}$ J is thermal energy at room temperature. If we use this formula to solve for the viscosity, we obtain $\eta \approx 2$ Pa·s. This is approximately 2000 times the viscosity of water, indicating that the chromosome domains at scale $R \approx 0.5$ μm have heavily constrained dynamics. The similarity for the timescales of redistribution of nucleoid proteins [40 s for Fis, Fig. 6; note a FRAP recovery time of ~80 s was measured for H-NS by Kumar *et al*. (2010)] to the structural correlation time suggests that the constraints that make the nucleoid shape fluctuations so slow are generated by proteins bound to the nucleoid, compacting and cross-linking it.

We also note that we have noticed a slight variation in the structure correlation time with growth condition. The origin of this variation may lie in the different replication dynamics and transcription patterns for these different growth conditions, and suggests directions for further study, e.g. dependence of the correlation time with drugs

that modify transcription, replication or translation, or on mutations that affect those processes or other aspects of chromosome dynamics.

Our general conclusion of a 'protein-cross-linked elastic filamentous' nucleoid is in accordance with the analysis of Wiggins *et al*. (2010), as well as with observations of coherent positioning dynamics of the nucleoid (Niki *et al*., 2000; Bates and Kleckner, 2005; Nielsen *et al*., 2006; 2007; Joshi *et al*., 2011). Given the variation in apparent condensation, geometrical shape and segregation of nucleoids in cells growing in minimal and rich media, it would be interesting to repeat the analysis of Wiggins in rapidly growing cells; it is plausible that locus fluctuations will be even smaller during rapid growth, reflecting a more rigid chromosome structure. It would be even more useful to use live-cell locus-tracking methods (Elmore *et al*., 2005; Fiebig *et al*., 2006; X. Wang *et al*., 2006; Espeli *et al*., 2008; Weber *et al*., 2010) to study enough tags at once (i.e. ~10), so as to determine the dynamics of local deformations along the chromosome, and to elucidate clearly the scale at which linear organization of loci gives way to, e.g. macrodomain structures (Thiel *et al*., 2012).

Experimental procedures

Bacterial strains and constructs

We used the *E. coli* strain FRAG1B: F^-, *rha*, *thi*, *gal*, $lacZ_{am}$, P_{N25}/*tetR*, P_{lacI}^Q/*lacI*, and Sp^R (Le *et al*., 2005), which contains a constitutively expressed chromosomal *lacI* gene and the wild-type chromosomal *fis* gene. FRAG1B cells were transformed with plasmid pZE12-*GFP–fis* carrying an IPTG-inducible *GFP–fis* gene fusion and ampicillin resistance. Plasmid pZE12-*GFP–fis* was constructed as follows: the *GFP–fis* gene fusion was amplified by PCR from plasmid pRJ2001 (Graham *et al*., 2011) and inserted between the KpnI and HindIII sites of the pBR322-derived plasmid pZE12 (Lutz and Bujard, 1997), resulting in the *GFP–fis* gene under control of a tightly regulated artificial PLlacO-1 promoter. The ectopically expressed *GFP–fis* enables controlled constitutive amounts of fluorescently tagged Fis to be synthesized in addition to native Fis, whose levels vary widely as a function of growth rate and growth phase (e.g. compare endogenous Fis levels in LB vs. M9 glycerol, Fig. S1). Enhanced green-fluorescent protein (eGFP) (F64L S65T) is inserted between amino acid residues 5 and 6 within the unstructured N-terminal peptide segment of Fis that is located on the opposite end of the polypeptide from the DNA-binding region. DNA-binding properties of GFP–Fis are very similar to Fis *in vitro* (Graham *et al*., 2011), and GFP–Fis promotes transcriptional activation [*proP P2* promoter (McLeod *et al*., 1999)], Hin-catalysed site-specific DNA inversion (Osuna *et al*., 1991), and phage lambda excision (Ball and Johnson, 1991) *in vivo*.

Growth conditions

Growth media used for these experiments were LB, minimal M9 and minimal AB medium, all containing 50 μg ml^{-1} ampicillin. AB minimal medium contained 0.2% glucose, 0.4% sodium-acetate and 1 μg ml^{-1} thiamine. M9 minimal medium contained 0.4% glycerol as the carbon source and was supplemented with 1 μg ml^{-1} thiamine. Cells were grown from a single colony overnight at 30°C, diluted 1:1000 into fresh medium, induced with IPTG (0.1–1 mM), and were harvested at an OD_{600} of 0.1 to perform microscopy experiments. For nucleoid positioning experiments, membrane dye FM4-64 was added to the liquid culture and the agarose gel at a final concentration of 1.5 μM.

Microscopy

A drop (3–5 μl) of cell culture was transferred onto a glass coverslip and then covered with 2–3% low melting point agarose pad prepared in the same medium containing the same concentrations of ampicillin and IPTG as the liquid culture. In order to produce the substrate with linear patterning with narrow grooves, the agarose gel was solidified on a diffraction grating (Newport 05RG300-3000-2) with 3 μm groove spacing. The prepared sample was placed on a heated objective at 30°C for imaging. Cells were imaged using a high-resolution wide-field fluorescence microscope [Olympus IX-81, 100×/1.45 NA objective, 1.6× magnifier slide, ImageEM EMCCD camera (Hamamatsu), and Coherent Sapphire 488 nm laser] with pixel size of 100 nm. The sample was illuminated with the laser at an angle of incidence slightly larger than the critical angle for TIRF (oblique illumination fluorescence), which allows for a larger depth of view in the area near the cover glass.

Data acquisition and analysis

Image acquisition and deconvolution was performed using SlideBook software (Olympus). The average time between every image (5 min for rapid growth and 10 min for slow growth) and exposure times (0.25 s exposure time for slow growth due to higher GFP–Fis expression and 0.5 s for rapid growth) at which the time-lapse images were taken were adjusted to minimize phototoxicity (cells were observed to divide for four generations with less ~10% increase in cell cycle time). Rapid sequence images were taken every 5–10 s with 0.25–0.5 s exposure time over 5 min. Z-stacks of images were collected with 0.2–0.3 μm step sizes, and then deconvolved using constrained iterative analysis (SlideBook, Olympus). The remaining image analyses for the fluorescence intensity and nucleoid positioning measurements, correlation, FRAP and writhe calculation analysis were performed using ImageJ software.

Correlation analysis

The stack of rapid sequence images was aligned by the Stackreg ImageJ plugin (Thevenaz *et al*., 1998) (http://bigwww.epfl.ch/thevenaz/stackreg/) to correct for drift. Each stack of nucleoid images was divided into five pixel-wide square regions for which the average autocorrelation coefficient of the mean intensity over time was calculated using the Correlation Coefficient Calculator ImageJ plugin of Tully and Rasband (http://shell.abtech.org/~tully/ImageJ/). The average

autocorrelation function for the nucleoid was then fit to an exponential with an offset using the Curve Fitting ImageJ plugin.

Nucleoid positioning measurements

Fluorescence images of the nucleoid and the membrane were superimposed for each cell. The intensity profile of the cell along its long axis was read by a MATLAB code to determine the position of the nucleoid with respect to the membrane; the nucleoid edges were determined as where the intensity of the nucleoid drops to half the intensity at the local maximum.

FRAP analysis

Photobleaching of the fluorescence in the region of interest (half of the nucleoid in one cell) for ~20 s was followed by post-bleach image sequences with one image recorded (with 0.25 s exposure time) every 15 s over 5 min. Fluorescence intensities of the bleached and unbleached regions were determined for every time point and were normalized to the intensity of the same region in the pre-bleach image. Intensity profile of the bleached area was then fitted to an exponential recovery using curve fitting plugin in ImageJ to determine the characteristic time of the recovery.

Writhe calculation analysis

Z-stacked images of the nucleoids were resliced perpendicular to the cell's long axis by the ImageJ Reslice plugin. The centre of intensity in each cross section was determined by finding the local maxima in each slice using the Find Local Maxima macro in ImageJ. As there were more than one local maximum in some slices, we determined the centre of mass in every slice as the centre of intensity. Reconstructing the 3D path for the nucleoid (a polygon with N segments) and the writhe calculation was performed by a custom MATLAB code using the method of Klenin and Langowski (2000).

Acknowledgements

We thank Professor Philippe Cluzel and Mr Lance Min for providing advice and materials. Jeannette Chau provided technical support. Work at NU was supported by NSF Grants DMR-0715099, MCB-1022117, DMR-1206868, DMR-0520513 and DMR-1121262 (NU-MRSEC), by NIH-NCI Grant U54CA143869-01 (NU-PS-OC) and by the Chicago Biomedical Consortium with support from the Searle Funds at the Chicago Community Trust. Work at UCLA was supported by NIH Grant GM038509.

References

Ali, B.M., Amit, R., Braslavsky, I., Oppenheim, A.B., Gileadi, O., and Stavans, J. (2001) Compaction of single DNA molecules induced by binding of integration host factor (IHF). *Proc Natl Acad Sci USA* **98:** 10658–10663.

Ball, C.A., and Johnson, R.C. (1991) Efficient excision of phage lambda from the *Escherichia coli* chromosome requires the Fis protein. *J Bacteriol* **173:** 4027–4031.

Bates, D., and Kleckner, N. (2005) Chromosome and replisome dynamics in *E. coli*: loss of sister cohesion triggers global chromosome movement and mediates chromosome segregation. *Cell* **121:** 899–911.

Berlatzky, I.A., Rouvinski, A., and Ben-Yehuda, S. (2008) Spatial organization of a replicating bacterial chromosome. *Proc Natl Acad Sci USA* **105:** 14136–14140.

Boeneman, K., Fossum, S., Yang, Y., Fingland, N., Skarstad, K., and Crooke, E. (2009) *Escherichia coli* DnaA forms helical structures along the longitudinal cell axis distinct from MreB filaments. *Mol Microbiol* **72:** 645–657.

Browning, D.F., Grainger, D.C., and Busby, S.J. (2010) Effects of nucleoid-associated proteins on bacterial chromosome structure and gene expression. *Curr Opin Microbiol* **13:** 773–780.

Cabrera, J.E., Cagliero, C., Quan, S., Squires, C.L., and Jin, D.J. (2009) Active transcription of rRNA operons condenses the nucleoid in *Escherichia coli*: examining the effect of transcription on nucleoid structure in the absence of transertion. *J Bacteriol* **191:** 4180–4185.

Cho, B.K., Knight, E.M., Barrett, C.L., and Palsson, B.O. (2008) Genome-wide analysis of Fis binding in *Escherichia coli* indicates a causative role for A-/AT-tracts. *Genome Res* **18:** 900–910.

Cooper, S., and Helmstetter, C.E. (1968) Chromosome replication and the division cycle of *Escherichia coli* B/r. *J Mol Biol* **31:** 519–540.

Cui, Y., Petrushenko, Z.M., and Rybenkov, V.V. (2008) MukB acts as a macromolecular clamp in DNA condensation. *Nat Struct Mol Biol* **15:** 411–418.

Dame, R.T., Wyman, C., and Goosen, N. (2000) H-NS mediated compaction of DNA visualised by atomic force microscopy. *Nucleic Acids Res* **28:** 3504–3510.

Dame, R.T., Noom, M.C., and Wuite, G.J. (2006) Bacterial chromatin organization by H-NS protein unravelled using dual DNA manipulation. *Nature* **444:** 387–390.

Dame, R.T., Kalmykowa, O.J., and Grainger, D.C. (2011) Chromosomal macrodomains and associated proteins: implications for DNA organization and replication in gram negative bacteria. *PLoS Genet* **7:** e1002123.

Daoud, M., and Degennes, P.G. (1977) Statistics of macromolecular solutions trapped in small pores. *J Phys* **38:** 85–93.

Deng, S., Stein, R.A., and Higgins, N.P. (2005) Organization of supercoil domains and their reorganization by transcription. *Mol Microbiol* **57:** 1511–1521.

Elmore, S., Muller, M., Vischer, N., Odijk, T., and Woldringh, C.L. (2005) Single-particle tracking of oriC-GFP fluorescent spots during chromosome segregation in *Escherichia coli*. *J Struct Biol* **151:** 275–287.

van den Ent, F., Amos, L.A., and Lowe, J. (2001) Prokaryotic origin of the actin cytoskeleton. *Nature* **413:** 39–44.

Espeli, O., Mercier, R., and Boccard, F. (2008) DNA dynamics vary according to macrodomain topography in the *E. coli* chromosome. *Mol Microbiol* **68:** 1418–1427.

Espeli, O., Borne, R., Dupaigne, P., Thiel, A., Gigant, E., Mercier, R., and Boccard, F. (2012) A MatP-divisome interaction coordinates chromosome segregation with cell division in *E. coli*. *EMBO J* **31:** 3198–3211.

Fiebig, A., Keren, K., and Theriot, J.A. (2006) Fine-scale time-lapse analysis of the biphasic, dynamic behaviour of

the two *Vibrio cholerae* chromosomes. *Mol Microbiol* **60:** 1164–1178.

de Gennes, P.G. (1979) *Scaling Concepts in Polymer Physics*. Ithaca, NY: Cornell University Press.

Graham, J.S., Johnson, R.C., and Marko, J.F. (2011) Concentration-dependent exchange accelerates turnover of proteins bound to double-stranded DNA. *Nucleic Acids Res* **39:** 2249–2259.

Grainger, D.C., Hurd, D., Goldberg, M.D., and Busby, S.J. (2006) Association of nucleoid proteins with coding and non-coding segments of the *Escherichia coli* genome. *Nucleic Acids Res* **34:** 4642–4652.

Jin, D.J., and Cabrera, J.E. (2006) Coupling the distribution of RNA polymerase to global gene regulation and the dynamic structure of the bacterial nucleoid in *Escherichia coli*. *J Struct Biol* **156:** 284–291.

Joshi, M.C., Bourniquel, A., Fisher, J., Ho, B.T., Magnan, D., Kleckner, N., and Bates, D. (2011) *Escherichia coli* sister chromosome separation includes an abrupt global transition with concomitant release of late-splitting intersister snaps. *Proc Natl Acad Sci USA* **108:** 2765–2770.

Jun, S., and Mulder, B. (2006) Entropy-driven spatial organization of highly confined polymers: lessons for the bacterial chromosome. *Proc Natl Acad Sci USA* **103:** 12388–12393.

Kahramanoglou, C., Seshasayee, A.S., Prieto, A.I., Ibberson, D., Schmidt, S., Zimmermann, J., *et al*. (2011) Direct and indirect effects of H-NS and Fis on global gene expression control in *Escherichia coli*. *Nucleic Acids Res* **39:** 2073–2091.

Klenin, K., and Langowski, J. (2000) Computation of writhe in modeling of supercoiled DNA. *Biopolymers* **54:** 307–317.

Kruse, T., Moller-Jensen, J., Lobner-Olesen, A., and Gerdes, K. (2003) Dysfunctional MreB inhibits chromosome segregation in *Escherichia coli*. *EMBO J* **22:** 5283–5292.

Kumar, M., Mommer, M.S., and Sourjik, V. (2010) Mobility of cytoplasmic, membrane, and DNA-binding proteins in *Escherichia coli*. *Biophys J* **98:** 552–559.

Le, T.T., Harlepp, S., Guet, C.C., Dittmar, K., Emonet, T., Pan, T., and Cluzel, P. (2005) *Proc Natl Acad Sci USA* **102:** 9160–9164.

Libby, E.A., Roggiani, M., and Goulian, M. (2012) Membrane protein expression triggers chromosomal locus repositioning in bacteria. *Proc Natl Acad Sci USA* **109:** 7445–7450.

Lim, C.J., Whang, Y.R., Kenney, L.J., and Yan, J. (2012) Gene silencing H-NS paralogue StpA forms a rigid protein filament along DNA that blocks DNA accessibility. *Nucleic Acids Res* **40:** 3316–3328.

Liu, Y., Chen, H., Kenney, L.J., and Yan, J. (2010) A divalent switch drives H-NS/DNA-binding conformations between stiffening and bridging modes. *Genes Dev* **24:** 339–344.

Lutz, R., and Bujard, H. (1997) Independent and tight regulation of transcriptional units in *Escherichia coli* via the LacR/O, the TetR/O and AraC/I1-I2 regulatory elements. *Nucleic Acids Res* **25:** 1203–1210.

McLeod, S.M., Xu, J., Cramton, S.E., Gaal, T., Gourse, R.L., and Johnson, R.C. (1999) Localization of amino acids required for Fis to function as a class II transcriptional activator at the RpoS-dependent proP P2 promoter. *J Mol Biol* **294:** 333–346.

Marko, J.F. (2009) Linking topology of tethered polymer rings with applications to chromosome segregation and estimation of the knotting length. *Phys Rev E Stat Nonlin Soft Matter Phys* **79:** 051905.

Marko, J.F. (2011) Scaling of linking and writhing numbers for spherically confined and topologically equilibrated flexible polymers. *J Stat Phys* **142:** 1353–1370.

Mason, D.J., and Powelson, D.M. (1956) Nuclear division as observed in live bacteria by a new technique. *J Bacteriol* **71:** 474–479.

Mercier, R., Petit, M.A., Schbath, S., Robin, S., El Karoui, M., Boccard, F., and Espeli, O. (2008) The MatP/matS site-specific system organizes the terminus region of the *E. coli* chromosome into a macrodomain. *Cell* **135:** 475–485.

Mondal, J., Bratton, B.P., Li, Y., Yethiraj, A., and Weisshaar, J.C. (2011) Entropy-based mechanism of ribosome-nucleoid segregation in *E. coli* cells. *Biophys J* **100:** 2605–2613.

Nielsen, H.J., Li, Y., Youngren, B., Hansen, F.G., and Austin, S. (2006) Progressive segregation of the *Escherichia coli* chromosome. *Mol Microbiol* **61:** 383–393.

Nielsen, H.J., Youngren, B., Hansen, F.G., and Austin, S. (2007) Dynamics of *Escherichia coli* chromosome segregation during multifork replication. *J Bacteriol* **189:** 8660–8666.

Niki, H., Yamaichi, Y., and Hiraga, S. (2000) Dynamic organization of chromosomal DNA in *Escherichia coli*. *Genes Dev* **14:** 212–223.

van Noort, J., Verbrugge, S., Goosen, N., Dekker, C., and Dame, R.T. (2004) Dual architectural roles of HU: formation of flexible hinges and rigid filaments. *Proc Natl Acad Sci USA* **101:** 6969–6974.

Osuna, R., Finkel, S.E., and Johnson, R.C. (1991) Identification of two functional regions in Fis: the N-terminus is required to promote Hin-mediated DNA inversion but not lambda excision. *EMBO J* **10:** 1593–1603.

Pelletier, J., Halvorsen, K., Ha, B.Y., Paparcone, R., Sandler, S.J., Woldringh, C.L., *et al*. (2012) Physical manipulation of the *Escherichia coli* chromosome reveals its soft nature. *Proc Natl Acad Sci USA* **109:** E2649–E2656.

Possoz, C., Junier, I., and Espeli, O. (2012) Bacterial chromosome segregation. *Front Biosci* **17:** 1020–1034.

Postow, L., Hardy, C.D., Arsuaga, J., and Cozzarelli, N.R. (2004) Topological domain structure of the *Escherichia coli* chromosome. *Genes Dev* **18:** 1766–1779.

Rimsky, S., and Travers, A. (2011) Pervasive regulation of nucleoid structure and function by nucleoid-associated proteins. *Curr Opin Microbiol* **14:** 136–141.

Shao, Y., Feldman-Cohen, L.S., and Osuna, R. (2008) Functional characterization of the *Escherichia coli* Fis-DNA binding sequence. *J Mol Biol* **376:** 771–785.

She, W., Wang, Q., Mordukhova, E.A., and Rybenkov, V.V. (2007) MukEF is required for stable association of MukB with the chromosome. *J Bacteriol* **189:** 7062–7068.

Shih, Y.L., Le, T., and Rothfield, L. (2003) Division site selection in *Escherichia coli* involves dynamic redistribution of Min proteins within coiled structures that extend between the two cell poles. *Proc Natl Acad Sci USA* **100:** 7865–7870.

Skoko, D., Yoo, D., Bai, H., Schnurr, B., Yan, J., McLeod, S.M., *et al*. (2006) Mechanism of chromosome compaction and looping by the *Escherichia coli* nucleoid protein Fis. *J Mol Biol* **364:** 777–798.

Stella, S., Cascio, D., and Johnson, R.C. (2010) The shape of the DNA minor groove directs binding by the DNA-bending protein Fis. *Genes Dev* **24:** 814–826.

Swinger, K.K., and Rice, P.A. (2004) IHF and HU: flexible architects of bent DNA. *Curr Opin Struct Biol* **14:** 28–35.

Tao, H., Bausch, C., Richmond, C., Blattner, F.R., and Conway, T. (1999) Functional genomics: expression analysis of *Escherichia coli* growing on minimal and rich media. *J Bacteriol* **181:** 6425–6440.

van Teeffelen, S., Wang, S., Furchtgott, L., Huang, K.C., Wingreen, N.S., Shaevitz, J.W., and Gitai, Z. (2011) The bacterial actin MreB rotates, and rotation depends on cell-wall assembly. *Proc Natl Acad Sci USA* **108:** 15822–15827.

Thevenaz, P., Ruttimann, U.E., and Unser, M. (1998) A pyramid approach to subpixel registration based on intensity. *IEEE Trans Image Process* **7:** 27–41.

Thiel, A., Valens, M., Vallet-Gely, I., Espeli, O., and Boccard, F. (2012) Long-range chromosome organization in *E. coli*: a site-specific system isolates the Ter macrodomain. *PLoS Genet* **8:** e1002672.

Toro, E., and Shapiro, L. (2010) Bacterial chromosome organization and segregation. *Cold Spring Harb Perspect Biol* **2:** a000349.

Valencia-Burton, M., Shah, A., Sutin, J., Borogovac, A., McCullough, R.M., Cantor, C.R., *et al*. (2009) Spatiotemporal patterns and transcription kinetics of induced RNA in single bacterial cells. *Proc Natl Acad Sci USA* **106:** 16399–16404.

Valkenburg, J.A., and Woldringh, C.L. (1984) Phase separation between nucleoid and cytoplasm in *Escherichia coli* as defined by immersive refractometry. *J Bacteriol* **160:** 1151–1157.

Viollier, P.H., Thanbichler, M., McGrath, P.T., West, L., Meewan, M., McAdams, H.H., and Shapiro, L. (2004) Rapid and sequential movement of individual chromosomal loci to specific subcellular locations during bacterial DNA replication. *Proc Natl Acad Sci USA* **101:** 9257–9262.

Vora, T., Hottes, A.K., and Tavazoie, S. (2009) Protein occupancy landscape of a bacterial genome. *Mol Cell* **35:** 247–253.

Wang, Q., Mordukhova, E.A., Edwards, A.L., and Rybenkov, V.V. (2006) Chromosome condensation in the absence of the non-SMC subunits of MukBEF. *J Bacteriol* **188:** 4431–4441.

Wang, W., Li, G.W., Chen, C., Xie, X.S., and Zhuang, X. (2011) Chromosome organization by a nucleoid-associated protein in live bacteria. *Science* **333:** 1445–1449.

Wang, X., Possoz, C., and Sherratt, D.J. (2005) Dancing around the divisome: asymmetric chromosome segregation in *Escherichia coli*. *Genes Dev* **19:** 2367–2377.

Wang, X., Liu, X., Possoz, C., and Sherratt, D.J. (2006) The two *Escherichia coli* chromosome arms locate to separate cell halves. *Genes Dev* **20:** 1727–1731.

Weber, S.C., Spakowitz, A.J., and Theriot, J.A. (2010) Bacterial chromosomal loci move subdiffusively through a viscoelastic cytoplasm. *Phys Rev Lett* **104:** 238102.

Wiggins, P.A., Cheveralls, K.C., Martin, J.S., Lintner, R., and Kondev, J. (2010) Strong intranucleoid interactions organize the *Escherichia coli* chromosome into a nucleoid filament. *Proc Natl Acad Sci USA* **107:** 4991–4995.

Xiao, B., Zhang, H., Johnson, R.C., and Marko, J.F. (2011) Force-driven unbinding of proteins HU and Fis from DNA quantified using a thermodynamic Maxwell relation. *Nucleic Acids Res* **39:** 5568–5577.

Zimmerman, S.B., and Murphy, L.D. (1996) Macromolecular crowding and the mandatory condensation of DNA in bacteria. *FEBS Lett* **390:** 245–248.

Zimmerman, S.B., and Trach, S.O. (1991) Estimation of macromolecule concentrations and excluded volume effects for the cytoplasm of *Escherichia coli*. *J Mol Biol* **222:** 599–620.

Supporting information

Additional supporting information may be found in the online version of this article.